Effects of Temperature on Corrosion Behavior of Reinforcements in Simulated Sea-Sand Concrete Pore Solution

buildings

MDPI

Article

Effects of Temperature on Corrosion Behavior of Reinforcements in Simulated Sea-Sand Concrete Pore Solution

Song Xia [1], Yaoming Luo [2,3], Yongqiang Li [2,3], Wei Liu [2,3], Xiaobo Ding [2,3,*] and Luping Tang [4]

[1] School of Civil Engineering and Architecture, West Anhui University, Lu'an 237010, China; xias@wxc.edu.cn
[2] School of Civil Engineering, Shenzhen University, Shenzhen 518060, China; 2060471017@email.szu.edu.cn (Y.L.); liyo@chalmers.se (Y.L.); liuwei@szu.edu.cn (W.L.)
[3] Guangdong Provincial Key Laboratory of Durability for Marine Civil Engineering, Shenzhen 518060, China
[4] Division of Building Technology, Chalmers University of Technology, 41296 Gothenburg, Sweden; tang.luping@chalmers.se
* Correspondence: dxxxxb@126.com

Abstract: The effects of temperature on the chloride-induced corrosion behavior of reinforcing steel in simulated sea-sand concrete pore solution are studied by means of linear polarization resistance. The results show that the E_{corr} (corrosion potential) and i_{corr} (corrosion current density) of the reinforcing steels are temperature and/or chloride concentration (C_{Cl})-related parameters. A linear correlation between E_{corr} and temperature and a natural logarithmic correlation between i_{corr} and C_{Cl} are observed. It is proved that the relationship between the corrosion rate and temperature follows the Arrhenius equation, whereas the activation energy of corrosion reaction increases with the increase of C_{Cl}.

Keywords: corrosion potential; corrosion current density; chloride concentration; temperature; sea-sand

Citation: Xia, S.; Luo, Y.; Li, Y.; Liu, W.; Ding, X.; Tang, L. Effects of Temperature on Corrosion Behavior of Reinforcements in Simulated Sea-Sand Concrete Pore Solution. *Buildings* **2022**, *12*, 407. https://doi.org/10.3390/buildings12040407

Academic Editor: Elena Ferretti

Received: 13 February 2022
Accepted: 25 March 2022
Published: 28 March 2022

1. Introduction

Reinforced concrete structures manufactured with sea-sand without a fresh water wash can be termed as "sea-sand houses" [1]. The usage of unwashed sea-sand is strictly limited by different countries, and it can only be used for concrete mixtures when its chloride content is lower than a specific value, such as 0.06% (referring to the weight percentage of dry sand) in China [2] and 0.024% in Japan [3]. However, the direct usage of unwashed sea-sand is commonly seen in practical engineering. Based on the information from on-site investigation, reinforcements embedded inside "sea-sand house" will deteriorate far before the designated service life [4–6], and this has been a key issue affecting the quality of structures in many marine regions [7]. It is well known that, due to the highly alkaline environment provided by cement hydration products, a passive film is formed on the reinforcing surface that inhibits the metal corrosion reaction and is referred to as the steady passivation state [8,9]. However, when concrete pH is reduced or the chloride concentration (C_{Cl}) reaches a critical level, the passive film will be broken, and corrosion is initiated [4,5]. Based on Tuutti's model [10], the corrosion of reinforcements in concrete usually can be divided into two stages: i.e., the initiation and the propagation stages (Figure 1a). However, providing that the chlorides introduced by sea-sands are higher than the threshold value, the corrosion of reinforcement may skip the first initiation stage and go to the second propagation stage immediately after concrete placement. This phenomenon could be called the sea-sand house corrosion model (Figure 1b).

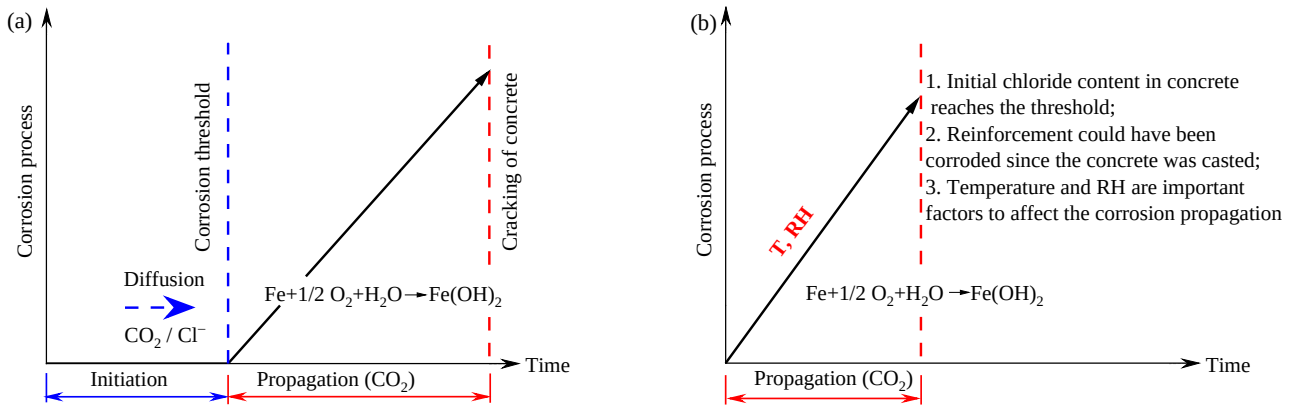

Figure 1. Schematic sketch of steel corrosion model in concrete: (**a**) Tuutti model [10]; (**b**) sea-sand house model.

For the chloride-induced corrosion of reinforcing steel in sea-sand concrete, temperature is an important factor influencing the corrosion behavior, and many studies have been conducted in this field [11–18]. However, due to the complexity of the corrosion process, results from different researchers have showed significant differences. Jiang [11], Liu [12] and Pan et al. [13] reported a continuous increase in corrosion rate along with elevated temperatures. Zivica et al. [14] and Alhozaimy et al. [15] agreed with this tendency but also found that corrosion rates decrease once the temperature exceeds 40 °C. In contrast, the results of Andrade et al. [16] and Michel et al. [17] showed no direct correlation between corrosion rate and temperature, while Lopez et al. [18] found that the corrosion rate of reinforcing steel decreases with increasing temperature. The different results reported in the latter three studies might be due to the lack of consideration of changes in water content in prepared samples, as the drying effect under the elevated temperature was not considered in their studies. In addition, the individual effect of chloride concentration on the corrosion behavior has been thoroughly studied by other researchers [19–25]. However, for concrete structures made with sea-sand, there should be no initiation stage of corrosion when the chloride content exceeds the threshold value. Both chloride content and temperature should be the key parameters to predict the degradation process of sea-sand concrete during its service life. Nevertheless, the chloride concentration is not thoroughly studied together with temperature as a combined influencing factor [15,26,27], which should be more important for the sea-sand concrete structure considering the widespread utilization of sea-sand for building construction in some coastal areas, such as cities in the south of China.

In order to solve the above-mentioned problems, experimental works, assessed by E_{corr} (corrosion potential) and i_{corr} (corrosion current density), were carried out in this study to explore the corrosion behavior of reinforcing steel in a simulated pore solution of sea-sand concrete under different chloride concentrations and temperatures. The relationship between the i_{corr} of reinforcing steel and temperature was then deduced with the Arrhenius equation. The activation energy of the reinforcing steel corrosion reaction and the pre-exponential factor with different C_{Cl} were obtained by calculation. A unified equation describing the relationship between the i_{corr}, temperature and C_{Cl} was also developed.

2. Experimental Program

In this study, HRB335 ribbed reinforcing steel with a diameter of Φ10 mm and a length of 220 mm was employed to represent the widely used reinforcing steel in practical engineering, and its chemical composition is given in Table 1.

Table 1. Composition of reinforcing steel (wt. %).

Fe	C	Mn	Si	P	S
98.96	0.21	0.63	0.17	0.005	0.026

Prior to immersion in chloride solution, oxide skins and corrosion artifacts on sample surfaces were removed following the method prescribed in RILEM TC 235 CTC [28], which can be briefly summarized as follows.

(a) The samples are immersed in acid solution, containing HCl (HCl: H_2O = 1:1 by volume) and urotropine (3 g/L).
(b) After a 2~3 min ultrasonic shower, oxide skins and surface corrosion are cleaned with a brush.
(c) The samples are rinsed with deionized water and are soaked in acetone solution for 2~3 s.
(d) Copper wire is welded at one end of each steel sample after drying.
(e) Both ends of each sample are coated with epoxy resin, leaving a 10 cm length uncoated (a sketch of the coating geometry is shown in Figure 2).

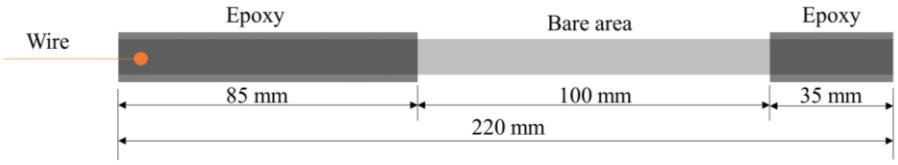

Figure 2. Schematic figure of a reinforcing steel sample.

In the experiment, saturated $Ca(OH)_2$ solution was used as the alkaline electrolyte solution to simulate concrete pore solution, which is thought to be close to the condition in actual pore solution [19,29–34]. To simulate a chloride-induced corrosion environment, NaCl was added to the simulated pore solution with concentrations ranging from 0.078~0.727 mol/L. All chemicals used in this experiment were analytical reagents, and distilled water was used as a solvent. To evaluate the influence of temperature on corrosion performance, the immersion solution was controlled in a constant temperature state during the experiment using a temperature-controlled water tank, which controlled the temperature varied in a range of 20~50 °C.

A three-electrode system, with Princeton Applied Research Model 283 Potentiostat/Galvanostat, as shown in Figure 3, was used for to measure the E_{corr} and i_{corr} of reinforcement in the simulated concrete pore solution. The reference electrode was a Leici 232/232-01-type saturated calomel electrode, the counter electrode was a Pt, the working electrode was the tested reinforcing steel, and the electrolyte solution was the simulated concrete pore solution. An example of linear polarization fitting is given in Figure 4. A linear equation, as shown in Equation (1), was used to fit the relationship between potential (y) and current (x).

$$y = ax + b \quad (1)$$

where a is fitted polarization resistance (Ω), and b is the fitted intercept.

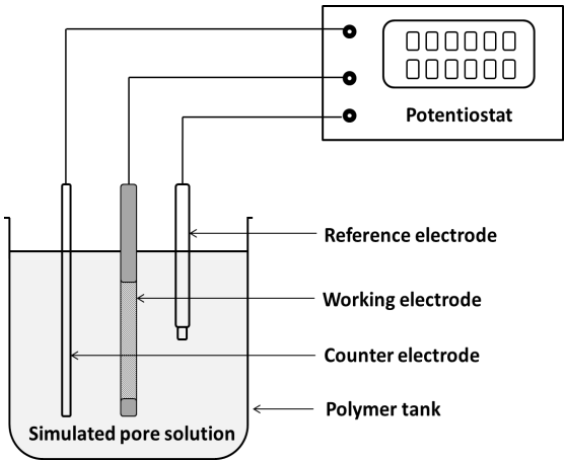

Figure 3. Schematic figure of the electrochemical test.

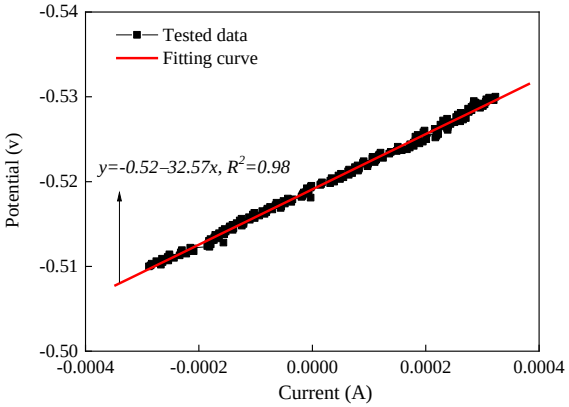

Figure 4. An example of linear polarization fitting.

Following ASTM G59 [35], the linear polarization scan was conducted with the sweeping range of −20~+20 mV with respect to open circuit potential at a scan rate of 0.166 mV/s. The open circuit potential was stabilized for 1 h before the start of each experiment.

3. Results and Analysis

3.1. Classical Testing Curve for Corrosion Potential and Corrosion Current Density

Figure 5 shows the variations of E_{corr} and i_{corr} as function of immersion duration in the simulated concrete pore solution, which is a saturated $Ca(OH)_2$ solution with and without chloride ions, respectively. It can be seen that the E_{corr} shifts upward and i_{corr} decreases with the immersion duration in the saturated pore solution without chlorides. In contrast, once the electrolyte contains chlorides, the E_{corr} shifts downward and i_{corr} increases with the immersion duration. The difference in the corrosion potential history between these two cases can be explained by the mixed potential theory. After 48 hours of immersion, the E_{corr} and i_{corr} reached a stable state. The purpose of conducting the electrochemical measurements after a period of immersion is to obtain a reliable result without other interferences [36–38]. Basically, the measurements should be applied until the OCP values are stabilized enough; e.g., less than 2 [39] or 5 mV [40] within 5 min. In our study, the records of corrosion potential and corrosion current density were performed after 48 hours of immersion. It was found that the variations of OCP values were within 3 mV from 24 to 48 h, which is quite stable in our view and the same as the procedure adopted by Lu et al. [41]. Therefore, the results after 48 hours of immersion presented in this study should be reliable and convincing.

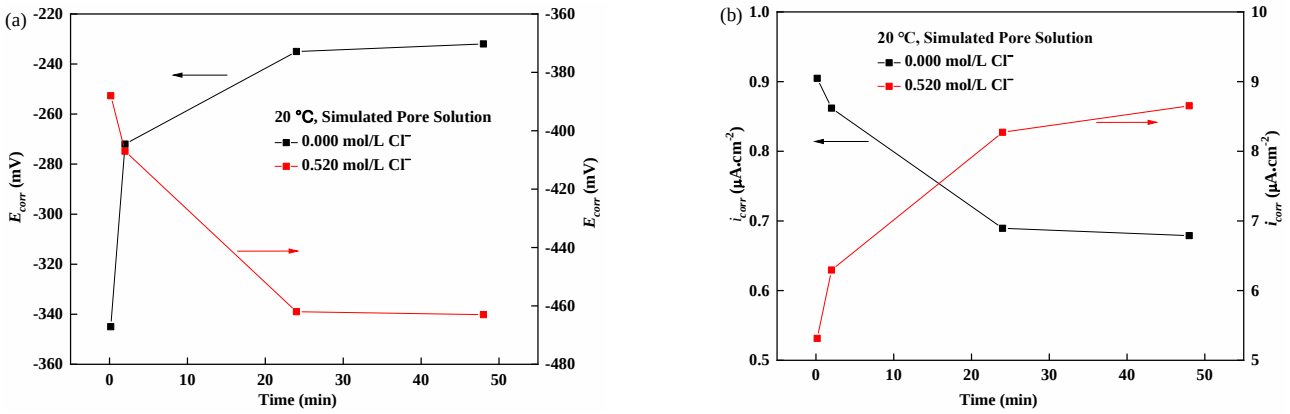

Figure 5. Developments of E_{corr} (**a**) and i_{corr} (**b**) during immersion in simulated concrete solution.

3.2. Corrosion Potential of Reinforcement at Different Temperatures and Chloride Concentrations

Figure 6 show the relationships of E_{corr} with the temperature and C_{Cl} in the simulated pore solution. As seen in Figure 6a, the Cl^- in the simulated pore solution lowered the E_{corr} of reinforcing steel obviously, to an extent of about 200~300 mV, and an increase of C_{Cl} also decreased the E_{corr}. When there was no Cl^- in the simulated pore solution, the value of E_{corr} of the reinforcing steel was roughly between −236 and –249 mV at the detected temperatures; in comparison, once Cl^- was present, the value was roughly between −405 and –573 mV. Based on the work of Hausmann [42], it can be inferred that the reinforcing steel is in the passivation state in the simulated solution without Cl^-, but in the activation state if the C_{Cl} equals to or is greater than 0.078 mol/L.

As seen in Figure 6b, there is a negative linear correlation between E_{corr} and temperature in the simulated pore solution, which is consistent with the tendency represented by the Nernst equation [14]. During the analysis, linear regressions of E_{corr} as a function of T are carried out in samples immersed by solutions with different C_{Cl} and the obtained coefficients (slopes and intercepts) are shown in Figure 7.

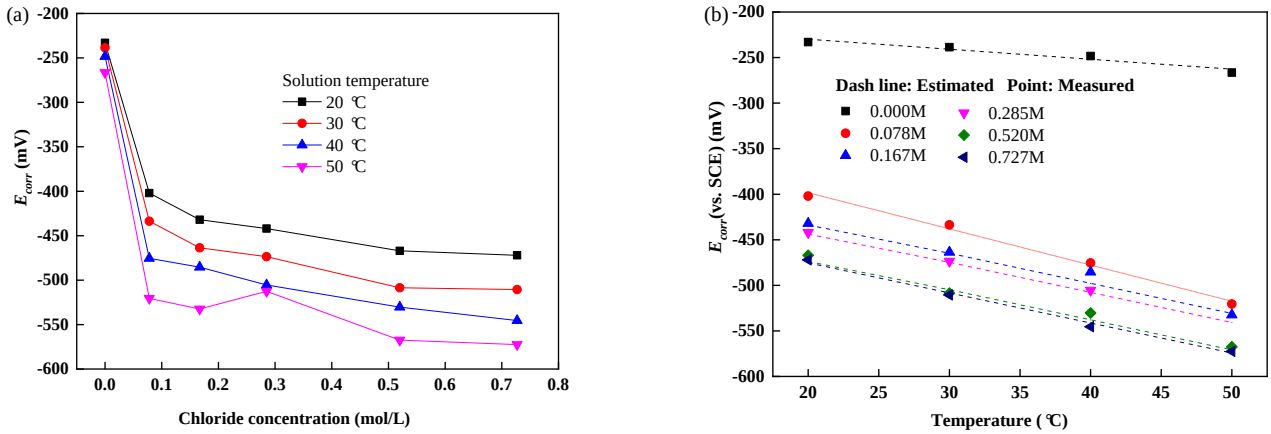

Figure 6. Effects of chloride concentration (**a**) and temperature (**b**) on the corrosion potential.

As can be seen from Figure 7a, the slope of the E_{corr}-T relationship in Figure 6b dramatically became negative at the condition of 0.072 mol/L Cl^- and then became relatively constant when C_{Cl} in the range of 0.167 to 0.727 mol/L. This could be the reason that Cl^- exceeding 0.167 mol/L exerts a significant influence on the behavior of metallic passivation and the anodic dissolution rate; however, Cl^- itself does not directly participate in the anodic oxidation or cathodic reduction reactions. So, the C_{Cl} has a negligible effect on the linear correlation of E_{corr}-T for Cl^- > 0.0167 mol/L. Figure 7b shows that the intercept of

the E_{corr}-T relationship, roughly obeying the exponential tendency, became more negative when C_{Cl} increased, implying severer corrosion at the higher temperature.

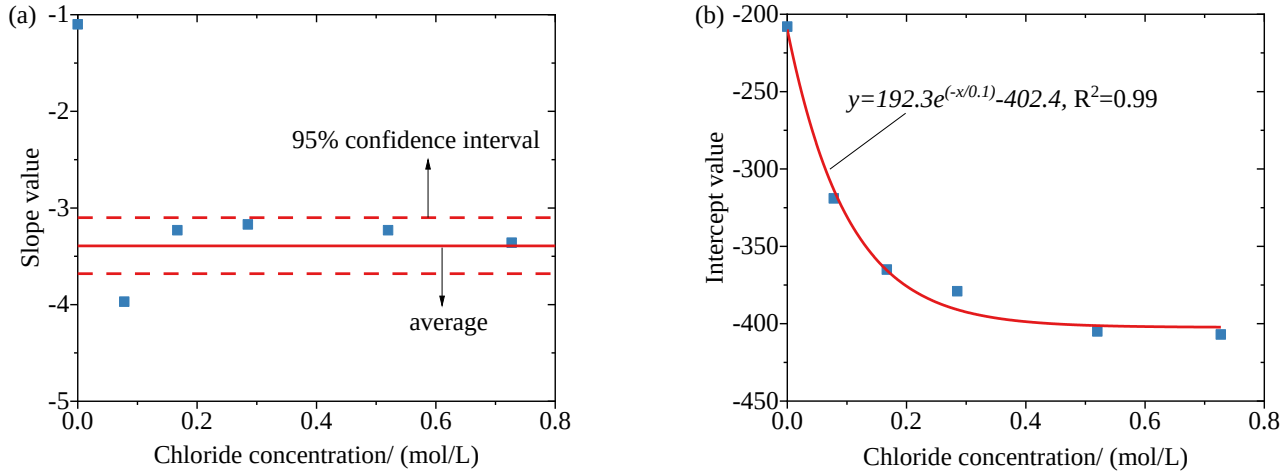

Figure 7. Regression coefficients of E_{corr}-T relationship: (**a**) slope; (**b**) intercept.

Given the linear relationship between E_{corr} and T, an empirical equation for the estimation of E_{corr} and T can be established irrespective of whether the reinforcing steel is in the activation or passivation state, as shown in Equation (2), which is valid within the temperature range of 20–50 °C.

$$E_{corr,T} - E_{corr,T_0} = k_T \times (T - T_0) \quad (2)$$

where T (°C) is the temperature of the solution; $E_{corr,T}$ and E_{corr,T_0} (mV) are the corrosion potentials of reinforcing steel at T (°C) and T_0 (°C), respectively; k_T is a constant with a value of 1.1 mV/°C for the passivation state and 3.3 mV/°C for the activation state (the average value for different C_{Cl}). Providing the corrosion potential of steel reinforcement at a certain temperature is known, the E_{corr} at other temperatures can be estimated based on Equation (2). Using T_0 = 20 °C as the reference temperature, a comparison between the measured and estimated values of the E_{corr} at different temperatures is illustrated in Figure 6b. All the relative errors between the measured and estimated values are less than 5%.

3.3. Corrosion Current Density of Reinforcements at Different Temperatures and Chloride Concentrations

Figure 8a shows the variation of i_{corr} with the C_{Cl} at different temperatures. It can be seen that the C_{Cl} has an obvious impact on the i_{corr} and a higher C_{Cl} resulting in a larger i_{corr}. With the increase of the C_{Cl} from 0.078 to 0.727 mol/L, the i_{corr} at different temperatures increases by more than double on average, which is a similar trend to that reported by peer researchers. Jiang et al. [43] and Yu et al. [44] proved that C_{Cl} has a limited effect on i_{corr} for reinforcing steel with a protective passive film, whereas significant effects were only found for reinforcing steel in the active state. The associations between i_{corr} and C_{Cl} may be related to the dissolution rate of the passive film [45] or the adsorption characteristics of Cl^- at the surface of reinforcing steel [46]. Moreover, as chloride ions are mainly in the anodic region, their effects on the anodic reaction are significant, which in turn influences the corrosion current [47].

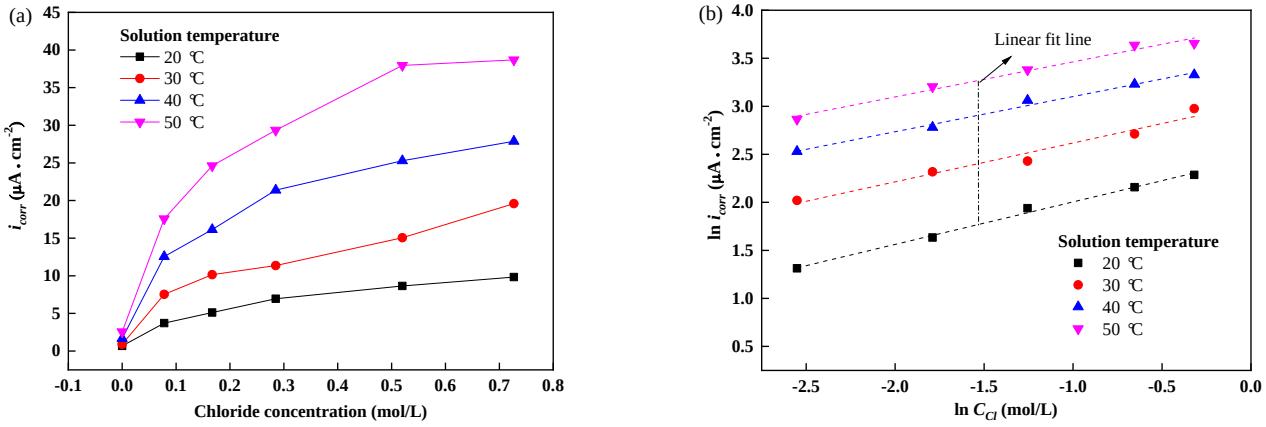

Figure 8. Relationship between current density and chloride concentration: (**a**) i_{corr} vs. C_{Cl}; (**b**) lni_{corr} vs. lnC_{Cl}.

During the analysis, it was found that there is a good linear relationship between natural logarithms of i_{corr} and C_{Cl}, as seen in Figure 8b. The corresponding equation can be expressed as Equation (3):

$$\ln i_{corr} = a_{Cl} + b_{Cl} \cdot \ln C_{Cl} \quad (3)$$

where a_{Cl} and b_{Cl} are the linear fitting coefficients, and C_{Cl} is the chloride concentration. This linear relationship between lni_{corr} and lnC_{Cl} was also reported by Abd El Aal et al. [45], who used simulated pore solution containing chlorides together with $Ca(OH)_2$. Figure 9 provides regression coefficients of a_{Cl} and b_{Cl}. It is obvious that both coefficients of a_{Cl} and b_{Cl} are temperature dependent and exponentially increased and decreased, respectively, with the increasing temperatures. Based on the theory of reaction kinetics, the electrode reaction speed (v) is linearly associated with the concentration of the electrode reactant (c), while according to Equation (3) obtained from experimental results, i_{corr} is natural logarithmically related to the C_{Cl}. Therefore, it can be deduced that Cl^- is not a reactant of the anode electrode reaction of metal anode dissolution; instead, it works as a catalyst for the corrosion reaction.

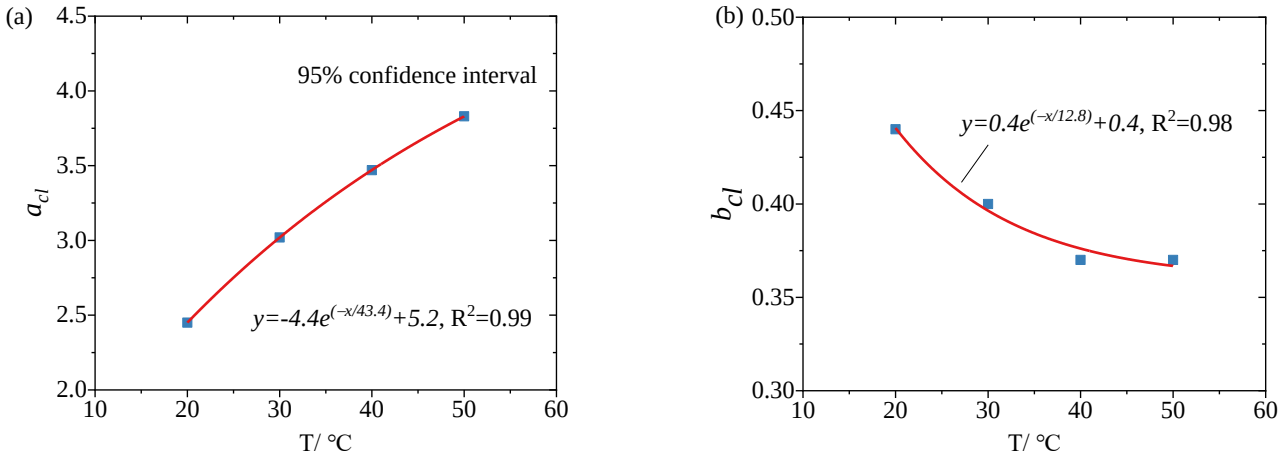

Figure 9. Regression coefficients of lni_{corr}-lnC_{Cl} relationship: (**a**) a_{Cl}; (**b**) b_{Cl}.

Figure 10 shows the influence of temperature on i_{corr} and the current density ratio ($i_{corr,T}/i_{corr,20}$). With an increase in temperature, the polarization resistance of reinforcing steel falls significantly, and the i_{corr} shows a clear increase. When the reinforcing steel is in the passivation state—i.e., without influence from Cl^-, an increase of 10 °C could lead to a further increase in i_{corr} by a factor of 1.3~1.8. This illustrates that temperature also has a significant influence on the corrosion rate of reinforcing steel in the passivation state, which

is consistent with the studies of Michel et al. [17]. In contrast, once the reinforcing steel is in the activated state, influenced by 0.078~0.727 mol/L of Cl^-, an increase of 10 °C could lead to a 1.4~1.9 times increase in i_{corr}. Therefore, the effect of temperature on the corrosion rate of reinforcing steel, in either passivated or activated state, makes limited difference, and the values are lower than the previous values from 2 to 4 times, as deduced according to Van't Hoff's rule [48].

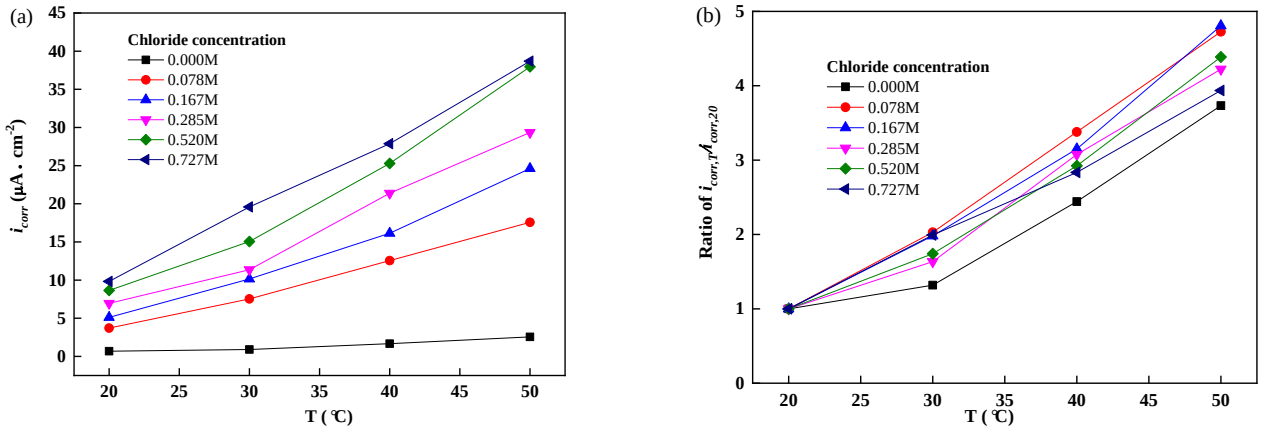

Figure 10. Relationship between current density and temperature: (**a**) i_{corr} vs. temperature; (**b**) ratio of $i_{corr,T}/i_{corr,20}$ vs. temperature.

Based on the Arrhenius equation [49,50], the dependence between the reaction rate constant (k) and T for reinforcing steel corrosion follows Equation (4).

$$k = A \cdot \exp\left(-\frac{E_a}{RT}\right) \tag{4}$$

where A is the pre-exponential factor ($mol^{-1} \cdot dm^3 \cdot s^{-1}$), E_a is the activation energy ($kJ \cdot mol^{-1}$), and R is the gas constant. For the electrode system of reinforcing steel corrosion, the value of k cannot be easily and directly measured. Instead, its mathematical relationship with i_{corr} can be derived from the Stern–Geary equation and Faraday's law, following the calculation as mentioned in Equations (4)–(9) listed below.

The relation between i_{corr} and polarization resistance R_P is expressed as Equation (5) [51,52]:

$$i_{corr} = B/R_P \tag{5}$$

where B is the Tafel constant, which can be determined based on Andrade and Gonzalez's work [53–55] and has the value of 26 mV. According to Faraday's law, the relationship between i_{corr} of the electrode reaction from metal anode dissolution and the electrode reaction rate can be calculated following Equation (6).

$$i_{corr} = nFv \tag{6}$$

where n is the stoichiometric coefficient of electrons in the electrode reaction, F is the Faraday constant, and v is the electrode reaction speed. When the electrode reaction proceeds in the direction of metal anode dissolution and the reaction is rate-limited by the charge migration step at the solid–liquid interface, the relationship between v and the concentration of electrode reactants c can be expressed as Equation (7).

$$v = kc \tag{7}$$

where k is the rate constant of the electrode reaction, as referenced in Equation (4). When the reactant is a metal atom, the value of c is unity (1 mol/cm^3). Substituting Equation (7) into Equation (6) yields

$$i_{corr} = nFkc \tag{8}$$

According to Equation (8), the reaction rate constant k can be calculated by using i_{corr} of the reinforcing steel. Substituting Equation (4) into Equation (8), the correlation equation between i_{corr} and temperature can be obtained as shown in Equation (9).

$$i_{corr} = nFcA \cdot \exp\left(-\frac{E_a}{RT}\right) \tag{9}$$

Taking the natural logarithm calculation of both sides of Equation (9), we find

$$\ln i_{corr} = \ln(nFcA) - \frac{E_a}{RT} \tag{10}$$

Consequently, the Arrhenius plots, as shown in Figure 11, can be obtained by plotting $\ln i_{corr}$ vs. $1/T$. As can be seen from the figure, there is a good linear relationship between these two parameters, which illustrates that the relationship between the corrosion rate of reinforcing steel and temperature conforms well with the Arrhenius equation at the temperature of 20~50 °C. Meanwhile, the result proves that the slop of the linear relationship ($-E_a$/R) is constant for each analysis, which means that the E_a is a temperature-independent factor for the corrosion of reinforcing steel.

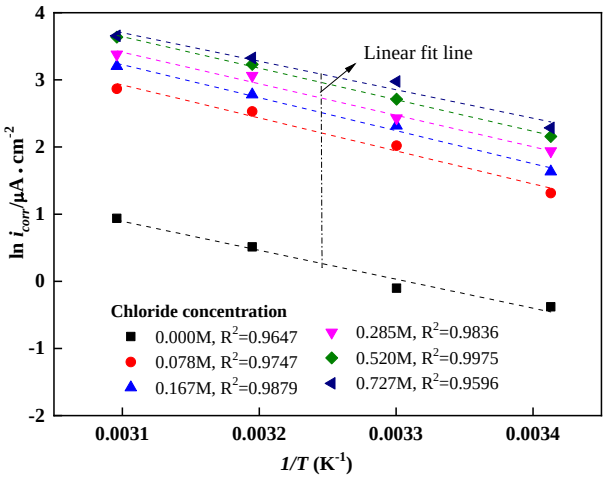

Figure 11. Arrhenius plots of the corrosion reaction with chloride concentration and temperature.

The values of E_a (kJ·mol^{-1}) and ln(A) (mol^{-1}·dm^3·s^{-1}) of the corrosion reaction of reinforcing steel in the simulated pore solutions with various C_{Cl} are shown in Figure 12. It can be known that E_a decreases with increases in C_{Cl}, providing the existence of Cl^-, and ranges from 35.8 and 41.5 kJ/mol, which is very close to the values of 35~40 kJ/mol, as presented by Michel et al. [17]. By discarding the value at 0 mol/L Cl^-, the relationship between E_a and chloride concentration seems unclear, as the value in 0.727 mol/L Cl^- has exceeded the 95% confidence interval. Further study is needed to study this relationship in wider ranges of chloride concentration. Regarding the ln(A), all of the fitted results with the existence of Cl^- are within the 95% confidence interval, which means that ln(A) could be seen as a constant in this condition.

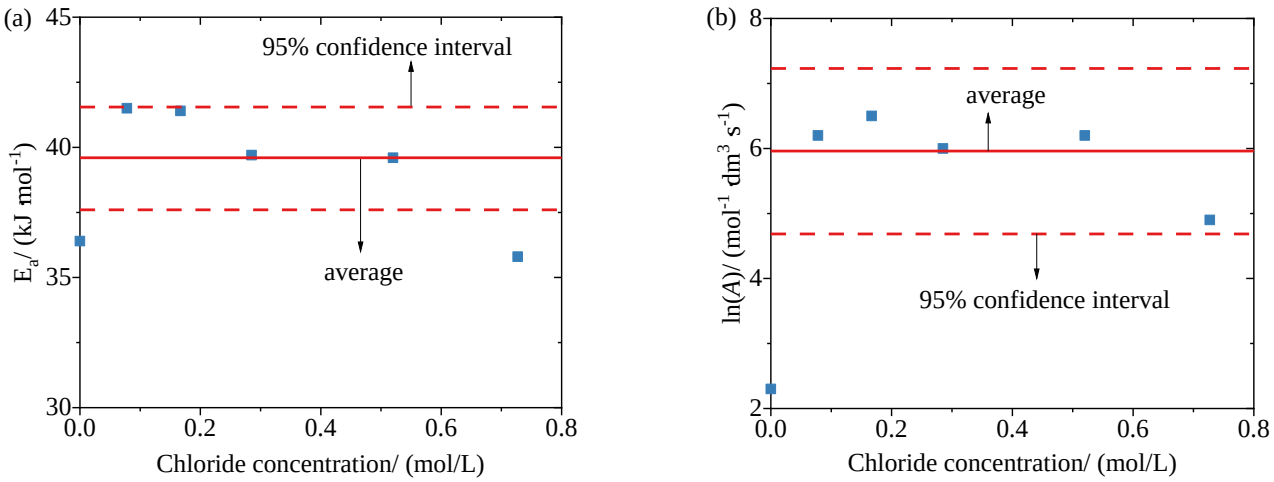

Figure 12. Regression coefficients of (**a**) Ea and (**b**) ln(*A*).

Additionally, as explained in the former paragraph, the value of E_a, or the "$-E_a$/R", reveals the sensitivity of the electrode reaction rate to the change in temperature. It can be assumed that the samples immersed in a higher concentration of chloride solution have a lower value of E_a and a corresponding lower temperature sensitivity. This is consistent with the results shown in Figure 10b: for the tests containing Cl^-, the highest increase rate of i_{corr} due to a change in temperature is in the sample with the lowest C_{Cl} (0.078 mol/L), for which the E_a is the highest.

According to the mathematical relationships between $\ln i_{corr}$, C_{Cl} and T, as described in Equations (2) and (9), a unified equation for the three variables can be deduced as the Equation (11):

$$\ln i_{corr} = a_{T,Cl} + b_{T,Cl} \cdot \ln C_{Cl} + c_{T,Cl} \cdot \frac{1}{T} \quad (11)$$

where $a_{T,Cl}$, $b_{T,Cl}$ and $c_{T,Cl}$ are constants. By a linear fitting of the $\ln C_{Cl}$, T and $\ln i_{corr}$, the values of $a_{T,Cl}$, $b_{T,Cl}$ and $c_{T,Cl}$ are obtained, which have the values of 18.4, 0.39 and -4691, respectively, and the coefficient of fitting R^2 is about 0.99. Therefore, the corrosion current density of the reinforcing steel in the simulated pore solution that has a chloride concentration and temperature can be determined based on the empirical relationship as shown in Equation (12).

$$\ln i_{corr} = 18.4 + 0.39 \cdot \ln C_{Cl} - 4691 \cdot \frac{1}{T} \quad (12)$$

4. Conclusions

In this paper, the effects of temperature on the chloride-induced corrosion behavior of reinforcing steel in simulated concrete pore solution are examined by means of linear polarization resistance (LPR). From the obtained results, the following conclusions can be drawn:

(1) There is an excellent linear correlation between E_{corr} and temperature. The slope of the linear correlation is related only to the corrosion state of the reinforcing steel—i.e., the passivation or activation—and this slope is independent of the chloride concentration C_{Cl} in the simulated pore solution.

(2) The chloride concentration in the simulated pore solution significantly affects i_{corr}. When the chloride concentration increases from 0.078 to 0.727 mol/L, i_{corr} values at different temperatures are more than doubled on average. There is a natural logarithmic correlation between i_{corr} and chloride concentration in the simulated pore solution.

(3) Temperature has a significant influence on i_{corr}. The relationship between corrosion rate and temperature T is found to be well described by an Arrhenius equation within the experimental temperature range. The activation energy E_a of the corrosion

reaction decreases with increasing chloride concentration in the simulated pore solution. However, there is no clear correlation between the pre-exponential factor *A* and chloride concentration.

(4) Although a big difference may exist between pore solution in concrete and simulated pore solution, the results obtained in this study could still be an indication of corrosion behavior of reinforcements in sea-sand concrete.

Author Contributions: Conceptualization, S.X. and Y.L. (Yaoming Luo); methodology, Y.L. (Yongqiang Li); validation, W.L.; formal analysis, W.L.; writing—original draft preparation, X.D.; writing—review and editing, X.D., Y.L. (Yongqiang Li) and L.T.; funding acquisition, S.X. and W.L. All authors have read and agreed to the published version of the manuscript.

Funding: This research was funded by the National Natural Science Foundation of China (51978408, 51978414, 51678368), the Natural Science Foundation of Anhui education department (Grant No. KJ2021A0952), the China Scholarship Council (202004190006), and the Guangdong Provincial Key Laboratory of Durability for Marine Civil Engineering (SZU) (2020B1212060074). The study has been partially supported by funding from the European Union's Horizon 2020 research and innovation program under the Marie Skłodowska-Curie grant agreement No 777823.

Data Availability Statement: The data is available for requesting.

Acknowledgments: We want to thank all the help from every colleague.

Conflicts of Interest: The authors declare no conflict of interest.

References

1. Hope, B.; Page, J.; Ip, A. Corrosion rates of steel in concrete. *Cem. Concr. Res.* **1986**, *16*, 771–781. [CrossRef]
2. *GB/T 14684-2011*; Sand for Construction. The General Administration of Quality Supervision Inspection and Quarantine and the Standardization Administration of the People's Republic of China: Beijing, China, 2011.
3. JIS A 5308; Ready-Mixed Concrete. 2009. Available online: https://www.wdfxw.net/doc34805001.htm (accessed on 13 February 2022).
4. Juenger, M.C.; Jennings, H.M. Effects of high alkalinity on cement pastes. *ACI Mater. J.* **2001**, *98*, 251–255.
5. Tang, S.; Yao, Y.; Andrade, C.; Li, Z. Recent durability studies on concrete structure. *Cem. Concr. Res.* **2015**, *78*, 143–154. [CrossRef]
6. Guo, M.; Hu, B.; Xing, F.; Zhou, X.; Sun, M.; Sui, L.; Zhou, Y. Characterization of the mechanical properties of eco-friendly concrete made with untreated sea sand and seawater based on statistical analysis. *Constr. Build. Mater.* **2020**, *234*, 117339. [CrossRef]
7. Page, C.; Treadaway, K. Aspects of the electrochemistry of steel in concrete. *Nature* **1982**, *297*, 109–115. [CrossRef]
8. Hou, D.; Zhang, K.; Hong, F.; Wu, S.; Wang, Z.; Li, M.; Wang, M. The corrosion deterioration of reinforced passivation film: The impact of defects. *Appl. Surf. Sci.* **2022**, *319*, 126142. [CrossRef]
9. Jin, Z.; Zhao, X.; Du, Y.; Yang, S.; Wang, D.; Zhao, T.; Bai, Y. Comprehensive properties of passive film formed in simulated pore solution of alkali-activated concrete. *Constr. Build. Mater.* **2022**, *319*, 126142. [CrossRef]
10. Tuutti, K. *Corrosion of Steel in Concrete*; Cement and Concrete Research Institute: Stockholm, Sweden, 1982; pp. 115–129. [CrossRef]
11. Jiang, J.H.; Yuan, Y.S. Development and prediction strategy of steel corrosion rate in concrete under natural climate. *Constr. Build. Mater.* **2013**, *44*, 287–292. [CrossRef]
12. Liu, T.; Weyers, R.W. Modeling the dynamic corrosion process in chloride contaminated concrete structures. *Cem. Concr. Res.* **1998**, *28*, 365–379. [CrossRef]
13. Pan, C.; Cui, Y.; Liu, L.; Guo, M.; Wang, Z. Effect of temperature on corrosion behavior of low-alloy steel exposed to a simulated marine atmospheric environment. *J. Mater. Eng. Perform.* **2020**, *29*, 1400–1409. [CrossRef]
14. Zivica, V.; Krajči, L.; Bagel, L.; Vargová, M. Significance of the ambient temperature and the steel material in the process of concrete reinforcement corrosion. *Constr. Build. Mater.* **1997**, *11*, 99–103. [CrossRef]
15. Alhozaimy, A.; Hussain, R.; Al-Zaid, R.; Al-Negheimish, A. Coupled effect of ambient high relative humidity and varying temperature marine environment on corrosion of reinforced concrete. *Constr. Build. Mater.* **2012**, *28*, 55–64. [CrossRef]
16. Andrade, C.; Alonso, C.; Sarría, J. Corrosion rate evolution in concrete structures exposed to the atmosphere. *Cem. Concr. Compos.* **2002**, *24*, 55–64. [CrossRef]
17. Michel, A.; Nygaard, P.V.; Geiker, M. Experimental investigation on the short-term impact of temperature and moisture on reinforcement corrosion. *Corros. Sci.* **2013**, *72*, 26–34. [CrossRef]
18. López, W.; González, J.A.; Andrade, C. Influence of temperature on the service life of rebars. *Cem. Concr. Res.* **1993**, *23*, 1130–1140. [CrossRef]
19. Shi, J.; Sun, W.; Jiang, J.; Zhang, Y. Influence of chloride concentration and pre-passivation on the pitting corrosion resistance of low-alloy reinforcing steel in simulated concrete pore solution. *Constr. Build. Mater.* **2016**, *111*, 805–813. [CrossRef]

20. Zhang, S.; Hou, L.; Du, H.; Wei, H.; Liu, B.; Wei, Y. A study on the interaction between chloride ions and CO_2 towards carbon steel corrosion. *Corros. Sci.* **2020**, *167*, 108531. [CrossRef]
21. Jin, S.H.; Yang, H.J.; Hwang, J.P.; Ann, K.Y. Corrosion behaviour of steel in CAC-mixed concrete containing different concentrations of chloride. *Constr. Build. Mater.* **2016**, *110*, 227–234. [CrossRef]
22. Feng, W.; Tarakbay, A.; Ali Memon, S.; Tang, W.; Cui, H. Methods of accelerating chloride-induced corrosion in steel-reinforced concrete: A comparative review. *Constr. Build. Mater.* **2021**, *289*, 123165. [CrossRef]
23. Noushini, A.; Castel, A.; Aldred, J.; Rawal, A. Chloride diffusion resistance and chloride binding capacity of fly ash-based geopolymer concrete. *Cem. Concr. Compos.* **2020**, *105*, 103290. [CrossRef]
24. Yu, Y.; Chen, X.; Gao, W.; Wu, D.; Castel, A. Modelling non-isothermal chloride ingress in unsaturated cement-based materials. *Constr. Build. Mater.* **2019**, *217*, 441–455. [CrossRef]
25. Yu, Y.; Gao, W.; Castel, A.; Chen, X.; Liu, A. An integrated framework for modelling time-dependent corrosion propagation in offshore concrete structures. *Eng. Struct.* **2021**, *228*, 111482. [CrossRef]
26. Alhozaimy, A.; Hussain, R.R.; Al-Negheimish, A.; Al-Zaid, R.; Singh, D.D.N. Effect of simulated concrete pore solution chemistry, chloride ions, and temperature on passive layer formed on steel reinforcement. *ACI Mater. J.* **2014**, *111*, 411–421. [CrossRef]
27. Hussain, R.R.; Ishida, T. Enhanced electro-chemical corrosion model for reinforced concrete under severe coupled action of chloride and temperature. *Constr. Build. Mater.* **2011**, *25*, 1305–1315. [CrossRef]
28. Tang, L.P.; Frederiksen, J.M.; Angst, U.; Polder, R.; Alonso, M.; Elsener, B.; Hooton, D.; Pacheco, J. Experiences from RILEM TC 235-CTC in recommending a test method for chloride threshold values in concrete. *RILEM Tech. Lett.* **2018**, *3*, 25–31. [CrossRef]
29. Bensabra, H.; Azzouz, N. Study of rust effect on the corrosion behavior of reinforcement steel using impedance spectroscopy. *Metall. Mater. Trans.* **2013**, *44*, 5703–5710. [CrossRef]
30. Saremi, M.; Mahallati, E. A study on chloride-induced depassivation of mild steel in simulated concrete pore solution. *Cem. Concr. Res.* **2002**, *32*, 1915–1921. [CrossRef]
31. Bautista, A.; Blanco, G.; Velasco, F. Corrosion behaviour of low-nickel austenitic stainless steels reinforcements: A comparative study in simulated pore solutions. *Cem. Concr. Res.* **2006**, *36*, 1922–1930. [CrossRef]
32. Alvarez, S.; Bautista, A.; Velasco, F. Corrosion behaviour of corrugated lean duplex stainless steels in simulated concrete pore solutions. *Corros. Sci.* **2011**, *53*, 1748–1755. [CrossRef]
33. Zheng, H.; Li, W.; Ma, F.; Kong, Q. The performance of a surface-applied corrosion inhibitor for the carbon steel in saturated $Ca(OH)_2$ solutions. *Cem. Concr. Res.* **2014**, *55*, 102–108. [CrossRef]
34. Williamson, J.; Isgor, O.B. The effect of simulated concrete pore solution composition and chlorides on the electronic properties of passive films on carbon steel rebar. *Corros. Sci.* **2016**, *106*, 82–95. [CrossRef]
35. *ASTM G59-97(2014)*; Standard Test Method for Conducting Potentiodynamic Polarization Resistance Measurements. West Conshohocken: Montgomery, PA, USA, 1967.
36. Zhao, Y.; Pan, T.; Yu, X.; Chen, D. Corrosion inhibition efficiency of triethanolammonium dodecylbenzene sulfonate on Q235 carbon steel in simulated concrete pore solution. *Corros. Sci.* **2019**, *158*, 108097. [CrossRef]
37. Zhi, F.; Jiang, L.; Jin, M.; Xu, P.; Xiao, B.; Jiang, Q.; Chen, L.; Gu, Y. Inhibition effect and mechanism of polyacrylamide for steel corrosion in simulated concrete pore solution. *Constr. Build. Mater.* **2020**, *259*, 120425. [CrossRef]
38. Qiu, J.; Li, Y.; Xu, Y.; Wu, A.; Macdonald, D.D. Effect of temperature on corrosion of carbon steel in simulated concrete pore solution under anoxic conditions. *Corros. Sci.* **2020**, *175*, 108886. [CrossRef]
39. Yang, H.; Li, W.; Liu, X.; Liu, A.; Hang, P.; Ding, R.; Li, T.; Zhang, Y.; Wang, W.; Xiong, C. Preparation of corrosion inhibitor loaded zeolites and corrosion resistance of carbon steel in simulated concrete pore solution. *Constr. Build. Mater.* **2019**, *225*, 90–98. [CrossRef]
40. Zhang, H.; Yan, Z.C.; Shen, K.C.; Chen, Q.; Zhang, L.C.; Li, X.Y.; Wang, W.M. Potentiodynamic and potentiostatic investigation on the passivation of Fe based glassy alloys in alkaline solution. *J. Alloys Compd.* **2021**, *857*, 157573. [CrossRef]
41. Lu, P.; Kursten, B.; Macdonald, D.D. Deconvolution of the Partial Anodic and Cathodic Processes during the Corrosion of Carbon Steel in Concrete Pore Solution under Simulated Anoxic Conditions. *Electrochim. Acta* **2014**, *143*, 312–323. [CrossRef]
42. Hausmann, D.A. Steel corrosion in concrete. *Mater. Prot.* **1967**, *6*, 19–23.
43. Jiang, L.; Huang, G.; Xu, J.; Zhu, Y.; Mo, L. Influence of chloride salt type on threshold level of reinforcement corrosion in simulated concrete pore solutions. *Constr. Build. Mater.* **2012**, *30*, 516–521. [CrossRef]
44. Yu, H.; Chiang, K.-T.; Yang, L. Threshold chloride level and characteristics of reinforcement corrosion initiation in simulated concrete pore solutions. *Constr. Build. Mater.* **2012**, *26*, 723–729. [CrossRef]
45. Abd El Aal, E.E.D.; Wanees, S.; Diab, A.; Abd El Haleem, S. Environmental factors affecting the corrosion behavior of reinforcing steel III. Measurement of pitting corrosion currents of steel in $Ca(OH)_2$ solutions under natural corrosion conditions. *Corros. Sci.* **2009**, *51*, 1611–1618. [CrossRef]
46. Jovic, V.; Jović, B. EIS and differential capacitance measurements onto single crystal faces in different solutions: Part I—Ag(111) in 0.01 M NaCl. *J. Electroanal. Chem.* **2003**, *541*, 1–11. [CrossRef]
47. Silva, N. Chloride induced Corrosion of Reinforcement Steel in Concrete-Threshold Values and Ion Distributions at the Concrete-Steel Interface. Ph.D. Thesis, Chalmers University of Technology, Gothenburg, Sweden, 2013; pp. 23–42.

48. Cohen Stuart, C.P. A Study of Temperature-Coefficients and Van't Hoff's Rule. Koninklijke Nederlandse Akademie van Wetenschappen Proceedings Series B Physical Sciences, 14, pp. 1159–1173. Available online: https://ui.adsabs.harvard.edu/abs/1912KNAB...14.1159C/abstract (accessed on 13 February 2022).
49. Popova, A.; Sokolova, E.; Raicheva, S.; Christov, M. AC and DC study of the temperature effect on mild steel corrosion in acid media in the presence of benzimidazole derivatives. *Corros. Sci.* **2003**, *45*, 33–58. [CrossRef]
50. Blasco-Tamarit, E.; Igual-Muñoz, A.; Antón, J.; García-García, D. Effect of temperature on the corrosion resistance and pitting behaviour of Alloy 31 in LiBr solutions. *Corros. Sci.* **2008**, *50*, 1848–1857. [CrossRef]
51. Stern, M.; Geary, A.L. Electrochemical polarization I. A theoretical analysis of the shape of polarization curves. *J. Electrochem. Soc* **1957**, *104*, 56–63. [CrossRef]
52. Stern, M. A method for determining corrosion rates from linear polarization pata. *Corrosion* **1958**, *14*, 60–64. [CrossRef]
53. Andrade, C. Quantitative measurements of corrosion rate of reinforcing steels embedded in concrete using polarization resistance measurement. *Mater. Corros.* **1978**, *29*, 515–519. [CrossRef]
54. Andrade, C.; Castelo, V.; Alonso, C.; Gonzalez, J.A. Corrosion effect of stray currents and the techniques for evaluating corrosion of rebars in concret. In *The Determination of the Corrosion Rate of Steel Embedded in Concrete by the Polarization Resistance and AC Impedance Methods*; ASTM Spec. Tech. Publ.: West Conshohocken, PA, USA, 1986; pp. 43–63. [CrossRef]
55. Gastaldi, M.; Bertolini, L. Effect of temperature on the corrosion behaviour of low-nickel duplex stainless steel bars in concrete. *Cem. Concr. Res.* **2014**, *56*, 52–60. [CrossRef]